# Oden Institute REPORT 20-19

## December 2020

# Dynamic fracture of brittle shells in a space-time adaptive isogeometric phase field framework

**by**

Karsten Paul, Thomas J.R. Hughes, Chad M. Landis and Roger A. Sauer

**Oden Institute for Computational Engineering and Sciences**
The University of Texas at Austin
Austin, Texas 78712

*Reference: Karsten Paul, Thomas J.R. Hughes, Chad M. Landis and Roger A. Sauer, "Dynamic fracture of brittle shells in a space-time adaptive isogeometric phase field framework," Oden Institute REPORT 20-19, Oden Institute for Computational Engineering and Sciences, The University of Texas at Austin, December 2020.*

# Dynamic fracture of brittle shells in a space-time adaptive isogeometric phase field framework

Karsten Paul, Thomas J.R. Hughes, Chad M. Landis and Roger A. Sauer

*Peter Wriggers has contributed immensely to the field of computational mechanics, and he has been a source of knowledge and inspiration to countless researchers. It was he who first brought me in touch with advanced fracture simulations, it was his textbook that first brought me in touch with shell finite elements, and it was he who first brought me in close touch with Tom Hughes. It is with gratitude that I dedicate this work to Peter Wriggers on the occasion of his 70th birthday. (Roger A. Sauer)*

**Abstract** Phase field models for fracture prediction gained popularity as the formulation does not require the specification of ad-hoc criteria and no discontinuities are inserted in the body. This work focuses on dynamic crack evolution of brittle shell structures considering large deformations. The energy contributions from in-plane and out-of-plane deformations are separately split into tensile and compressive components and the resulting coupled system is discretized within the isogeometric

Paul, K.
RWTH Aachen University, Aachen Institute for Advanced Study in Computational Engineering Science (AICES), Aachen, Germany
e-mail: paul@aices.rwth-aachen.de

Hughes, T.J.R.
The University of Texas at Austin, Oden Institute for Computational Engineering and Sciences, Austin, USA
e-mail: hughes@oden.utexas.edu

Landis, C.M.
The University of Texas at Austin, Department of Aerospace Engineering and Engineering Mechanics, Austin, USA
e-mail: landis@utexas.edu

Sauer, R.A.
RWTH Aachen University, Aachen Institute for Advanced Study in Computational Engineering Science (AICES), Aachen, Germany
Gdańsk University of Technology, Faculty of Civil and Environmental Engineering, Gdańsk, Poland
Indian Institute of Technology Kanpur, Department of Mechanical Engineering, Kanpur, India
e-mail: sauer@aices.rwth-aachen.de

analysis framework. The resulting system is solved fully monolithically and adaptive local refinement is used in space and time.

## 1 Introduction

Thin-walled structures are characterized by low weight and high strength, making them interesting for many engineering designs. Especially for high slenderness ratios, these shells can be modeled based on the assumptions of Kirchhoff-Love theory. In these, no rotational degrees-of-freedom (dofs) are used, but only displacement dofs are considered. The resulting equation of motion thus, includes fourth-order derivatives. Isogeometric analysis [10] is used to obtain the required $C^1$-continuity in the corresponding weak form. In this work, the shell formulation of [7] is used.

The prediction of fracture and failure is of crucial importance for the design of engineering structures. Phase field models for the prediction of fracture gained popularity as they do not require ad-hoc criteria and do not insert discontinuities in the body, e.g. in the displacement field. Phase field models for brittle fracture are based on the theory of Griffith [9] and its variational reformulation as an energy minimization problem [8]. An additive energy split is required to model the anisotropic behavior of crack evolution, i.e. such that there occurs no cracking in compression. The membrane and bending energies are split separately and the split based on surface stretches [1] is employed for the split of the membrane part. Based on the idea of [12], the bending energy is decomposed based on thickness integration, but here, the split is also based on surface stretches [14]. The resulting formulation allows for large deformations and avoids the expensive computations of spectral decompositions. A higher-order fracture energy [2] is employed. The small length scale parameter of the phase field is resolved by using local spatial refinement based on LR NURBS [6, 17] and the mesh is adaptively refined during the computation [14]. The resulting discretized coupled system is implicitly integrated in time using an adaptive time-stepping scheme and a monolithic solution approach. Patch constraints are used to allow for multi-patch discretizations [13].

## 2 Fracture of deforming surfaces

The mapping $\boldsymbol{x} = \boldsymbol{x}(\xi^\alpha, t)$ is used to describe a curved surface $\mathcal{S}$. Here, $\xi^\alpha$, $\alpha = 1, 2$ are the convected coordinates and $t$ denotes time. Based on this mapping, a co- and contra-variant basis can be associated to each surface point, i.e. $\{\boldsymbol{a}_\alpha, \boldsymbol{n}\}$ and $\{\boldsymbol{a}^\alpha, \boldsymbol{n}\}$, with covariant tangent vectors $\boldsymbol{a}_\alpha = \partial \boldsymbol{x}/\partial \xi^\alpha$, surface normal $\boldsymbol{n} = (\boldsymbol{a}_1 \times \boldsymbol{a}_2)/||\boldsymbol{a}_1 \times \boldsymbol{a}_2||$, and contra-variant tangent vectors $\boldsymbol{a}^\alpha = a^{\alpha\beta}\boldsymbol{a}_\beta$.

The co- and contra-variant surface metrics are given by $a_{\alpha\beta} = \boldsymbol{a}_\alpha \cdot \boldsymbol{a}_\beta$ and $[a^{\alpha\beta}] = [a_{\alpha\beta}]^{-1}$. Using the second parametric derivative $\boldsymbol{a}_{\alpha,\beta} = \boldsymbol{x}_{,\alpha\beta} = \partial \boldsymbol{a}_\alpha/\partial \xi^\beta$, the surface curvature is described via $b_{\alpha\beta} = \boldsymbol{a}_{\alpha,\beta} \cdot \boldsymbol{n}$.

## 2.1 Thin shell theory

The equation of motion can be written as [7]

$$\boldsymbol{T}^{\alpha}_{;\alpha} + \boldsymbol{f} = \rho\dot{\boldsymbol{v}} \quad \text{on } \mathcal{S}\times(0,\bar{T})\,, \tag{1}$$

with traction vector $\boldsymbol{T}^{\alpha}$, surface force $\boldsymbol{f}$ and final time $\bar{T}$. The stresses and moments follow from constitution. Here, hyperelastic material behavior is assumed and the elastic energy density is given by

$$\Psi_{\mathrm{el}}(a_{\alpha\beta}, b_{\alpha\beta}) = \Psi_{\mathrm{mem}}(a_{\alpha\beta}) + \Psi_{\mathrm{bend}}(b_{\alpha\beta})\,, \tag{2}$$

with the membrane energy density being composed of dilatational and deviatoric contributions, i.e. $\Psi_{\mathrm{mem}} = \Psi_{\mathrm{dil}} + \Psi_{\mathrm{dev}}$, where [16]

$$\Psi_{\mathrm{dil}} = \frac{K}{4}\left(J^2 - 1 - 2\,\ln J\right)\,, \quad \text{and} \quad \Psi_{\mathrm{dev}} = \frac{G}{2}\left(I_1/J - 2\right)\,. \tag{3}$$

Here, $I_1 := A^{\alpha\beta}a_{\alpha\beta}$ is the first invariant of the surface Cauchy-Green strain tensor and $J := \sqrt{\det[A^{\alpha\beta}]\det[a_{\alpha\beta}]}$ is the surface stretch.[1] Using $b_0^{\alpha\beta} = A^{\alpha\gamma}b_{\gamma\delta}A^{\beta\delta}$, the bending energy in (2) is given by [5]

$$\Psi_{\mathrm{bend}} = \frac{c}{2}\Big(b_{\alpha\beta} - B_{\alpha\beta}\Big)\Big(b_0^{\alpha\beta} - B^{\alpha\beta}\Big)\,. \tag{4}$$

## 2.2 Brittle fracture

The phase field $\phi = \phi(\xi^{\alpha}, t) \in [0,1]$ ranges from the undamaged state ($\phi = 1$) to the fully fractured state ($\phi = 0$). Phase evolution is described by a partial differential equation, which stems from the minimization of the Helmholtz free energy

$$\Pi_{\mathrm{int}} = \int_{\mathcal{S}_0} \Psi\,\mathrm{d}A = \int_{\mathcal{S}_0}\Big[g(\phi)\,\mathcal{H} + \Psi_{\mathrm{el}}^{-} + \Psi_{\mathrm{frac}}\Big]\,\mathrm{d}A\,. \tag{5}$$

The higher-order fracture energy density in (5) is given by [2, 14]

$$\Psi_{\mathrm{frac}} = \frac{\mathcal{G}_{\mathrm{c}}}{4\ell_0}\Big[(\phi-1)^2 + 2\ell_0^2\,\nabla_{\mathrm{S}}\phi\cdot\nabla_{\mathrm{S}}\phi + \ell_0^4\,(\Delta_{\mathrm{S}}\phi)^2\Big]\,, \tag{6}$$

with fracture toughness $\mathcal{G}_{\mathrm{c}}$ and length scale $\ell_0$ of the phase field model. The surface gradient and Laplacian are indicated by $\nabla_{\mathrm{S}}$ and $\Delta_{\mathrm{S}}$, respectively. The degradation of the bulk material is described by the cubic degradation function [3]

$$g(\phi) = (3-s)\phi^2 - (2-s)\phi^3\,, \quad \text{with } s = 10^{-4}\,. \tag{7}$$

[1] Quantities on the reference surface are either indicated by the subscript '0' or by a capital symbol.

Irreversibility of the fracture process is ensured by keeping track of the *fracture driving energy* by means of the history field

$$\mathcal{H}(\boldsymbol{x},t) := \max_{\tau\in[0,t]} \Psi^+_{\mathrm{el}}(\boldsymbol{x},\tau) \; . \tag{8}$$

The ‘positive’ and ‘negative’ energies in (5) and (8) are based on the additive energy split

$$\Psi_{\mathrm{el}} = \Psi^+_{\mathrm{el}} + \Psi^-_{\mathrm{el}} \,, \quad \text{with} \quad \Psi^\pm_{\mathrm{el}} = \Psi^\pm_{\mathrm{mem}} + \Psi^\pm_{\mathrm{bend}} \,, \tag{9}$$

which splits the energy into a part that contributes to crack evolution (‘+’), and a part that does not (‘-’). The contributions are given by [1, 14]

$$\Psi^+_{\mathrm{mem}} = \begin{cases} \Psi_{\mathrm{dev}} + \Psi_{\mathrm{dil}} \,, & J \geq 1 \\ \Psi_{\mathrm{dev}} \,, & J < 1 \end{cases} , \qquad \Psi^-_{\mathrm{mem}} = \begin{cases} 0 \,, & J \geq 1 \\ \Psi_{\mathrm{dil}} \,, & J < 1 \end{cases} , \tag{10}$$

and

$$\Psi^\pm_{\mathrm{bend}} = \int_{-\frac{T}{2}}^{\frac{T}{2}} \xi^2 \frac{12}{T^3} \frac{c}{2} \,\mathrm{tr}\big(\boldsymbol{K}^2\big)\, \mathcal{X}^\pm\big(\tilde{J}(\xi)\big)\,\mathrm{d}\xi \,, \quad \text{with} \quad \mathcal{X}^+\big(\tilde{J}(\xi)\big) = \begin{cases} 1 \,, & \tilde{J}(\xi) \geq 1 \,, \\ 0 \,, & \tilde{J}(\xi) < 1 \,, \end{cases} \tag{11}$$

and $\mathcal{X}^-\big(\tilde{J}(\xi)\big)$ analogously. In (11), $\boldsymbol{K} = (b_{\alpha\beta} - B_{\alpha\beta})\,\boldsymbol{A}^\alpha \otimes \boldsymbol{A}^\beta$ denotes the relative curvature tensor, $T$ is the shell thickness, and $\tilde{J} = \sqrt{\det[\tilde{A}^{\alpha\beta}]\,\det[\tilde{a}_{\alpha\beta}]}$ is the surface stretch of a shell layer [7]. Using the Euler-Lagrange equation and standard arguments of variational calculus, the strong form of the fracture framework is given by

$$\begin{cases} 2\ell_0/\mathcal{G}_{\mathrm{c}}\, g'(\phi)\,\mathcal{H} + \phi - 1 - 2\,\ell_0^2\,\Delta_{\mathrm{S}}\phi + \ell_0^4\,\Delta_{\mathrm{S}}\big(\Delta_{\mathrm{S}}\phi\big) = 0 & \text{on } \mathcal{S}\times(0,\bar{T}) \,, \\ \Delta_{\mathrm{S}}\phi = 0 & \text{on } \partial\mathcal{S}\times(0,\bar{T}) \,, \\ \nabla_{\mathrm{S}}\big(\ell_0^4\,\Delta_{\mathrm{S}}\phi - 2\,\ell_0^2\,\phi\big)\cdot\boldsymbol{\nu} = 0 & \text{on } \partial\mathcal{S}\times(0,\bar{T}) \,, \\ \phi = \phi_0 & \text{on } \mathcal{S}\times 0 \,. \end{cases} \tag{12}$$

## 2.3 Computational aspects

Isogeometric analysis [10] is used to obtain the required $C^1$-continuity in the weak formulations of (1) and (12), also see [14]. LR NURBS [6, 17] are used to allow for local refinement, such that the small length scale of the model ($\ell_0$) can be resolved properly. The FE mesh is adaptively refined based on the phase field: If a control value fulfills $\phi < 0.975$, all elements that lie in the support domain of the corresponding basis function will be flagged for refinement. The refinement is performed using the *structured mesh* strategy [11, 14].

The generalized-$\alpha$ method [4] is used for temporal discretization and the discretized coupled system is solved within a monolithic Newton-Raphson scheme. In experiments, it has been shown that the crack tip velocity stays below 60% of the Rayleigh wave speed $c_{\mathrm{R}}$ [15], such that a physical upper bound can be imposed on the time step, i.e. $\Delta t \leq \Delta t_{\max} < \Delta x_{\min}/(0.6\, c_{\mathrm{R}})$, where $\Delta x_{\min}$ denotes the minimum element length. The time step is adjusted based on the number of required Newton-Raphson iterations $n_{\mathrm{NR}}$ during the previous time step, i.e.

$$\Delta t_{n+1} = \begin{cases} 1.5\, \Delta t_n\,, & n_{\mathrm{NR}} < 4\,, \\ 1.1\, \Delta t_n\,, & n_{\mathrm{NR}} = 4\,, \\ 0.5\, \Delta t_n\,, & n_{\mathrm{NR}} > 4\,, \\ 0.2\, \Delta t_n\,, & \text{local spatial refinement}\,. \end{cases} \tag{13}$$

## 3 Numerical examples

The material parameters $K$, $G$ and $c$ in (3)–(4) are set like in [14]. Crack patterns are visualized by means of a red ($\phi = 0$) to blue ($\phi = 1$) colorscale. Further, the non-dimensionaliztion scheme by [14] is adopted such that all quantities are normalized by the reference time $T_0$, length $L_0$ and stiffness $E_0$.

### 3.1 Crack propagation around obstacles

This example investigates dynamic crack branching, kinking and deflection in a square two-dimensional domain. The initial state is shown in Fig. 1 and a displacement is imposed on the top edge upwards, and on the bottom edge downwards. Branching and kinking is achieved by locally increasing the fracture toughness by a factor of 10 in the two shown regions. The parameters are $\ell_0 = 0.0025\, L_0$, $\mathcal{G}_{\mathrm{c}} = 0.001\, E_0\, L_0$, $E = 100\, E_0$, $\nu = 0.3$, and the displacement increment is $\Delta\bar{u} = \bar{v}\Delta t$ with $\bar{v} = 0.0025\, L_0\, T_0^{-1}$. Crack evolution is illustrated in Fig. 2. The crack branches at the first reinforced area and is deflected in vertical direction. The two branches then kink toward the horizontal direction and start branching. The top crack is again

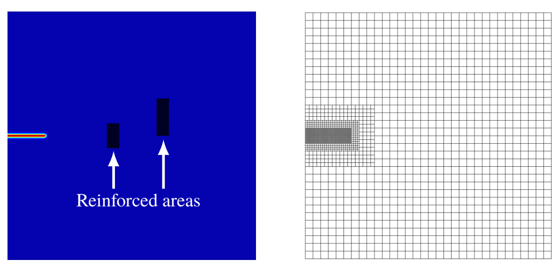


**Fig. 1** Crack propagation around obstacles: Initial phase field and initial LR mesh. The dark colored rectangles mark the regions of increased fracture toughness. The initial mesh consists of 32 × 32 elements and three local refinement levels are used.

deflected at the reinforced area and stops propagating shortly after the bottom crack reaches the right edge. The time step sizes according to (13) and the final adaptively locally refined mesh are shown in Fig. 3. Large time steps are used when there is no crack propagation and only the regions close to the cracks are refined.

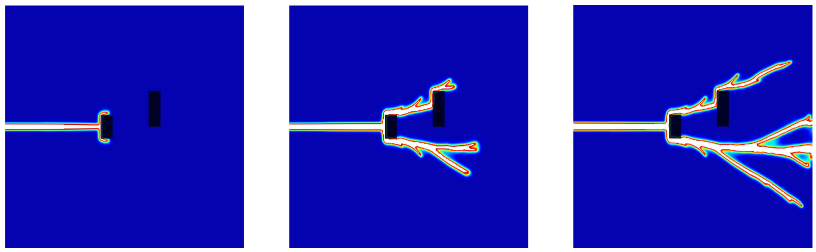

(a) $t \approx 2.98\,T_0$ (b) $t \approx 3.09\,T_0$ (c) $t \approx 3.20\,T_0$

**Fig. 2** Crack propagation around obstacles: Crack pattern at different snapshots. Regions with $\phi < 0.01$ are not visualized.

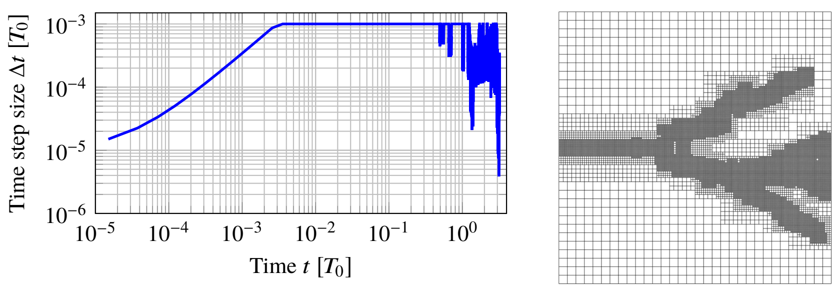


**Fig. 3** Crack propagation around obstacles: Adaptivity in time (left) and space (right, final LR mesh).

## 3.2 Fracturing balloon

This section investigates crack evolution on a spherical geometry that is imposed to the internal pressure $p(\phi) = 0.1\,E_0\,L_0^{-1}\phi$. The geometry is composed of six patches, as shown in Fig. 4 on the left (patch interfaces are indicated by the cyan-colored lines). Quadratic NURBS are used within each patch, and $C^1$-continuity across patch interfaces is restored by imposing patch constraints with the Lagrange multiplier (LMM) (constant interpolation) or the penalty method (PM), which is further elaborated in [13]. The radius is $L_0$ and the parameters are $\ell_0 = 0.015\,L_0$, $\mathcal{G}_c = 0.0005\,E_0\,L_0$, $E = 10\,E_0$, $\nu = 0.3$, $T = 10^{-4}L_0$, and bending stiffness $c =$

$10^{-5} E_0 L_0^2$. The elastic and fracture energies ($\Pi_{\text{el}}$ and $\Pi_{\text{frac}}$, respectively) over time

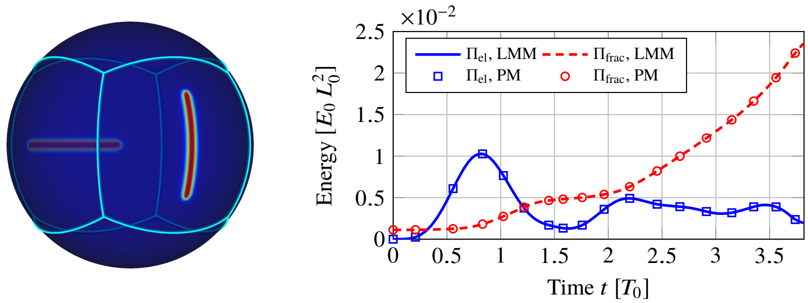


**Fig. 4** Fracturing balloon: Initial state with patch interfaces (left) and energy-time-curves (right).

for the two enforcement techniques are shown in Fig. 4 on the right. Crack evolution is visualized in Fig. 5. The cracks start branching and merge at the end. The first drop of the elastic energy occurs after the onset of crack propagation, and the last occurs when the geometry is fully fractured. Excellent agreement between the two enforcement techniques is achieved.

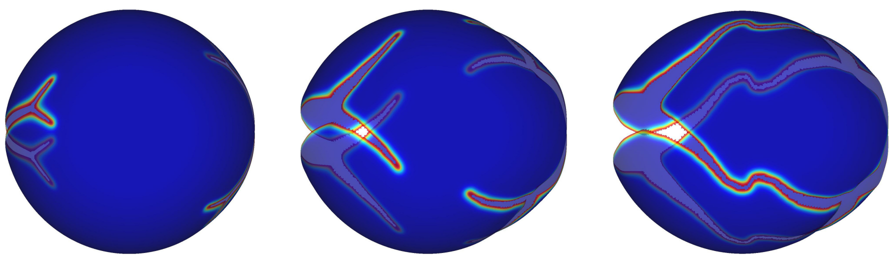

(a) $t \approx 1.6\,T_0$ (b) $t \approx 3.16\,T_0$ (c) $t \approx 3.81\,T_0$

**Fig. 5** Fracturing balloon: Crack pattern at different snapshots (visualized transparently). Regions with $\phi < 0.005$ are not visualized.

## 4 Conclusion

A dynamic phase field fracture framework for thin shells within a convective coordinate system is presented. Isogeometric analysis is used to obtain the required $C^1$-continuity in the weak form and LR NURBS are used for the local refinement. Adaptivity in space and time and the monolithic coupling of both PDEs ensures the efficient computation of complicated crack patterns, including branching, merging, kinking and deflection. This framework is further extended to consider geometries that are composed of multiple patches.

**Acknowledgements** The authors acknowledge funding by the Deutsche Forschungsgemeinschaft (DFG, German Research Foundation) – 33849990/GRK2379 (IRTG Modern Inverse Problems). Simulations were performed with computing resources granted by RWTH Aachen University under project rwth0625. Chad M. Landis and Thomas J.R. Hughes acknowledge support from ONR and Coreform through the Office of Naval Research grant N00014-17-1-2039 and the Department of Defense, Navy, Contract N6833518C0014.

## References

1. Amor, H., Marigo, J.-J., Maurini, C. (2009) Regularized formulation of the variational brittle fracture with unilateral contact: Numerical experiments. J Mech Phys Solids 57(8):1209–1229
2. Borden, M. J., Hughes, T. J. R., Landis, C. M., Verhoosel, C. V. (2014) A higher-order phase-field model for brittle fracture: Formulation and analysis within the isogeometric analysis framework. Comput Methods Appl Mech Eng 273:100–118
3. Borden, M. J., Hughes, T. J. R., Landis, C. M., Anvari, A., Lee, I. J. (2016) A phase-field formulation for fracture in ductile materials: Finite deformation balance law derivation, plastic degradation, and stress triaxiality effects. Comput Methods Appl Mech Eng 312:130–166
4. Chung, J., Hulbert, G. M. (1993) A time integration algorithm for structural dynamics with improved numerical dissipation: The generalized-alpha method. J Appl Mech 60(2):371–375
5. Ciarlet, P. G. (1993). Mathematical Elasticity: Three Dimensional Elasticity. North-Holland
6. Dokken, T., Lyche, T., Pettersen, K. F. (2013) Polynomial splines over locally refined box-partitions. Comput Aided Geom Des 30(3):331–356
7. Duong, T. X., Roohbakhshan, F., Sauer, R. A. (2017) A new rotation-free isogeometric thin shell formulation and a corresponding continuity constraint for patch boundaries. Comput Methods Appl Mech Eng 316:43–83.
8. Francfort, G., Marigo, J.-J. (1998). Revisiting brittle fracture as an energy minimization problem. J Mech Phys Solids 46(8):1319–1342
9. Griffith, A. A. (1921) VI. The Phenomena of Rupture and Flow in Solids. Philosophical Transactions of the Royal Society of London Series A 221:163–198
10. Hughes, T. J. R., Cottrell, J. A., Bazilevs, Y. (2005) Isogeometric analysis: CAD, finite elements, NURBS, exact geometry and mesh refinement. Comput Methods Appl Mech Eng 194(39–41):4135–4195
11. Johannessen, K. A., Kvamsdal, T., Dokken, T. (2014) Isogeometric analysis using LR B-splines. Comput Methods Appl Mech Eng 269:471–514
12. Kiendl, J., Ambati, M., De Lorenzis, L., Gomez, H., Reali, A. (2016) Phase-field description of brittle fracture in plates and shells. Comput Methods Appl Mech Eng 312:374–394
13. Paul, K., Zimmermann, C., Duong, T. X., Sauer, R. A. (2020) Isogeometric continuity constraints for multi-patch shells governed by fourth-order deformation and phase field models. Comput Methods Appl Mech Eng 370:113219
14. Paul, K., Zimmermann, C., Mandadapu, K. K., Hughes, T. J. R., Landis, C. M., Sauer, R. A. (2020) An adaptive space-time phase field formulation for dynamic fracture of brittle shells based on LR NURBS. Comput Mech 65:1039–1062.
15. Ravi-Chandar, K., Knauss, W. G. (1984) An experimental investigation into dynamic fracture: III. On steady-state crack propagation and crack branching. Int J Fract 26(2):141–154
16. Sauer, R. A., Duong, T. X. (2017) On the theoretical foundations of thin solid and liquid shells. Math Mech Solids 22(3):343–371
17. Zimmermann, C., Sauer, R. A. (2017) Adaptive local surface refinement based on LR NURBS and its application to contact. Comput Mech 60:1011–1031